공학석사학위논문

Solar energy conversion by the regular array of TiO_2 nanotubes anchored with ZnS/CdSSe/CdS quantum dots formed by sequential ionic bath deposition

TiO_2나노튜브에 SILAR방법으로 ZnS/CdSSe/CdS양자점을 도입한 태양전지 연구

2013년 2월

서울대학교 융합과학기술대학원

나노 융합 학과

박 수 정

Solar energy conversion by the regular array of TiO_2 nanotubes anchored with ZnS/CdSSe/CdS quantum dots formed by sequential ionic bath deposition

TiO_2나노튜브에 SILAR방법으로 ZnS/CdSSe/CdS양자점을 도입한 태양전지 연구

지도교수 이 성 훈

이 논문을 공학석사 학위논문으로 제출함.

2013년 2월

서울대학교 융합과학기술대학원
나노융합학과
박 수 정

박수정의 공학석사 학위논문을 인준함.

2013년 2월

위 원 장 _____ (인)

부위원장 _____ (인)

위 원 _____ (인)

Abstract

Solar energy conversion by the regular array of TiO_2 nanotubes anchored with ZnS/CdSSe/CdS quantum dots formed by sequential ionic bath deposition

Park, Soo Jeong
School of Conversion Science and Technology
The Graduate School
Seoul National University

The photoelectrode fabricated with the regular array of TiO_2 nanotubes anchored with ZnS/CdSSe/CdS quantum dots was prepared by the following steps: 1) the formation of the regular array of TiO_2 nanotubes on Ti metal, 2) the surface treatment of the TiO_2 nanotubes with $TiCl_4$ for the removal of surface defect sites, 3) the sequential deposition of CdS, CdSSe, and ZnS, in situ, onto the channel walls of TiO_2 nanotubes by the successive ionic layer adsorption and reaction (SILAR) procedure. The tuning the band gap of CdSSe was done in terms of controlling the composition of Cd, S, or Se during the SILAR procedure. In this way, a ladder-like energy structure suitable for carrier transfer was attained from ZnS/CdSSe/CdS through TiO_2 nanotubes to a Ti metal sheet. The more photoinduced charge carriers were generated and transferred from the anchored quantum dots to the TiO_2 nanotubes and thus, the solar

energy

conversion efficiency was enahnced. The power conversion efficiency (PCE) of our solar cell fabricated with the regular array of TiO_2 nanotubes anchored with CdSSe/CdS or CdSe/CdS quantum dots was PCE = 3.49 % and 2.81 % under the illumination at 100 mW/cm^2, respectively. To protect the photocorrosion of our solar cell photoanode from the electrolyte and to prevent the recombination, ZnS was introduced onto CdS/CdSSe. The power conversion efficiency (PCE) of our solar cell with the structure of a photoanode electrode, (ZnS/CdSSe/CdS/ TiO_2 NTs/ a Ti metal sheet) was 4.67 % under the illumination at 100 mW/cm^2.

Key words: *TiO_2 nanotubes, quantum dots, SILAR, Solar Cell*

Student number: 2009-22461

Table of Contents

List of Scheme

List of Table

List of Figure

CdSSe, and ZnS.) sensitized TiO_2 NTs photoelectrode..

CHAPTER 1. Backgrounds and Objective

Recently, Semiconductor sensitized solar cells are selected as one of the most promising alternative energy sources and attracted great attention as the third-generation photovoltaic device. The formation of anodic TiO_2 nanotubes has been widely investigated because of a wide range of applications such as photocatalysis, photoelectrodes, supercapacitors, hydrogen generators, and solar cells [1, 2]. For the application of TiO_2 for the solar cell, however, TiO_2 itself has less efficient because it (band gap E_g~3.2eV) captures only the UV portion of sunlight (4% of the whole solar emission [3]. Therefore, to enhance the solar energy conversion efficiency, we need to extend the solar energy absorption as much as possible through the visible to IR region. Firstly, the creation of impurity states near the valence band edge (O 2p character) or the conduction band edge (Ti 3d(t_{2g}) character) of TiO_2 by doping it with non-metal anions such as C [4], N [5], and S [6] or with transition metal cations such as Fe^{3+}, V^{4+} [7] , Mn^{2+}, Ni^{2+},and Cr^{3+} [8], respectively, can extend the absorption

to longer wavelengths (i.e. the visible region:~50% of the whole solar emission). Secondly, semiconductor QDs with band gaps lying in the visible or IR spectral range such as CdS [9], CdSe [10], CdTe [11], and PbS [12], are attached to the channel wall of the regular array of TiO_2 nanotubes in order to extend the solar energy absorption to the visble or IR [13]. Previously, Yuh-Lang Lee and other researchers reported that they achieved a maximum solar energy conversion efficiency of 4.22% with the CdSe/CdS/TiO_2 photoelectrode [14]. In particular, with ternary CdSSe alloy composition modulated, we can adjust the absorption wavelength of CdSSe in the visible region from blue to red [15-18]. There are two well-known methods to deposit the colloidal QDs layer on mesoporous metal oxides such as TiO_2. One approach is to presynthesize colloidal QDs surface-passivated with ligands and then to join them through linker molecules or electrostatic interaction with metal oxide surfaces [19-21]. The other is the direct growth of QD layers on metal oxide surfaces in situ through chemical bath deposition (CBD) [22] or

successive ionic layer adsorption and reaction(SILAR) [23-25]. However, at most, 14% of surface of nanoporous TiO_2 film was anchored with QDs through linkers or directly adsorbed with presynthesized colloidal QDs [26]. In the SILAR method using Na_2SeO_3, Se^{2-} is slowly released in the presence of Cd^{2+} and is poorly controlled[27]. The SILAR using SeO_2 instead of Na_2SeO_3 is carried out for the better deposition of metal selenides [24]. In the SILAR method, cationic and anionic precursors are dissolved in separate vessels. For one deposition cycle, the photoelectrode with the regular array of TiO_2 nanotubes is dipped into the precursor solution containing the metal cation. After rinsing excess precursors and drying them off, the photoelectrode is dipped into the second precursor solution containing the anion, and a second rinsing step completes the deposition cycle. The average QD size deposited onto the photoelectrode with the regular array of TiO_2 nanotubes can be controlled by the number of deposition cycles.

CHAPTER 2. Introduction

In this study, the photoelectrode fabricated with the regular array of TiO_2 nanotubes(NTs) anchored with ZnS(outer)/CdSSe/CdS(closer to TiO_2 NTs) quantum dots was prepared by the following steps: 1) the formation of the regular array of TiO_2 nanotubes on Ti metal, 2) the surface treatment of the TiO_2 nanotubes with $TiCl_4$ for the removal of surface defect sites, 3) the sequential deposition of CdS, CdSSe, and ZnS, in situ, onto the channel walls of TiO_2 nanotubes by the successive ionic layer adsorption and reaction (SILAR) procedure. A ladder-like energy structure suitable for carrier transfer was attained from ZnS/CdSSe/CdS through TiO_2 nanotubes to a Ti metal sheet. The more photoinduced charge carrier transfer from the quantum dots anchored on the TiO_2 nanotubes was achieved and thus, the solar energy conversion efficiency was enahnced. The power conversion efficiency (PCE) of our solar cell fabricated with the regular array of TiO_2 nanotubes anchored with CdSSe/CdS or CdSe/CdS quantum dots was PCE = 3.49 % and 2.81 % under the

illumination at 100 mW/cm^2, respectively. To protect the photocorrosion of our solar cell from the electrolyte and to prevent the recombination, ZnS was introduced onto CdSSe/CdS [28,30].

The power conversion efficiency (PCE) of our solar cell with the structure of a photoelectrode, (ZnS/CdSSe/CdS/TiO_2 NTs/ a Ti metal sheet) was **4.67 %** under the illumination at 100 mW/cm^2.

CHAPTER 3. Experimental

3.1. Materials

Titanium foil (0.25 mm thickness, 99.6 % purity, Goodfellow, England), ammonium fluoride (NH_4F, Junsei Chemical Co., 97.0 %), ethylene glycol (Samchun Chemical Co., 99.5 %), cadmium nitrate tetrahydrate ($Cd(NO_3)_2 \cdot 4H_2O$, Junsei Chemical Co., 98.0 %), sodium sulfide pentahydrate ($Na_2S \cdot 5H_2O$, Yakuri pure, 98.0 %), sodium sulfide (Na_2S, Sigma-Aldrich, 98.0 %), selenium dioxide (SeO_2, Sigma-Aldrich, 98.0 %), zinc sulfate heptahydrate ($ZnSO_4 \cdot 7H_2O$, Daejung chemical Co., 99.0 %), ethyl alcohol (C_2H_5OH, Dusan Chemical Co., 99.9 %), titanium (IV) chloride solution ($TiCl_4$, Sigma-Aldrich), 4-mercaptobenzoic acid ($C_7H_6O_2S$, Sigma-Aldrich, 99.0 %), and sodium sulfite heptahydrate ($Na_2SO_3 \cdot 7H_2O$, Junsei Chemical Co., 95.0 %) were used as received

3.2. Fabrication of array of TiO_2 NTs on a flat Ti sheet

The growth of TiO_2 nanotubes was done in ethylene glycol containing 0.7 wt% NH_4F and 2 vol % H_2O electrolyte at 25°C by anodizing Ti foil (0.25mm thickness, 99.6 % purity, Goodfellow, England) with the application of 60V DC (N5753A model, Agilent) for 2 h, as shown in Figure3.1. Ti foil was prepared as follows: washed with ethanol and acetone, followed by conventional oven-dry at 50°C. The vertically aligned array of TiO_2 nanotubes just grown was annealed at 450°C for 1h under ambient air condition to improve their crystallinity [31].

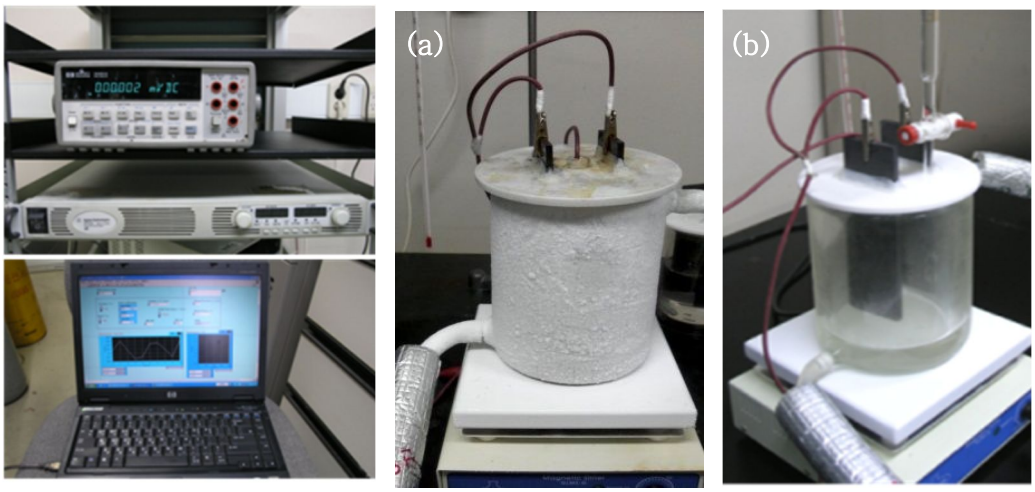

Fig 3.1 An experimental set up for (a) electropolishig and (b) anodizing of titanium.

3.3. $TiCl_4$ Treatment on the TiO_2 NTs

To improve the structural quality and to remove surface defect sites of the grown TiO_2 nanotubes, we dipped anatase TiO_2 nanotubes in 30mL of 5mM $TiCl_4$ aqueous solution and then took it out and kept it in an oven for 150 min at 50°C. We took it out and then washed it with deionized (DI) water and dried it in an oven at 90°C for 30min. We finally annealed it at 450°C for 1h under ambient air condition. The digital images of TiO_2 nanotubes untreated and treated with $TiCl_4$, were shown in Figure 4.1.

3.4. SILAR procedure for the growth of CdS, CdSSe, CdSe, and ZnS layers.

The optimized regular array of TiO_2 nanotubes surface-treated with $TiCl_4$ was alternatively soaked in two different solutions to deposit CdS: in

0.50M Cd $(NO_3)_2 \cdot 4H_2O$ dissolved in DI water for 3min and then in 0.50M $Na_2S \cdot 5H_2O$ dissolved in DI water. It was rinsed in DI water and acetone for 1min to remove excess precursors. This kind of cycle was repeated 20 times (denoted with "CdS20"). The average QD size deposited onto the regular array of TiO_2 nanotubes was controlled by the number of deposition cycles.

To deposit CdSSe ternary alloy subsequently next to CdS layer, the SILAR cycle was performed with 0.60M Cd $(NO_3)_2 \cdot 4H_2O$ dissolved in ethanol, 0.20M Na_2S dissolved in methanol/ethanol (7:3 v:v), and 0.30M SeO_2 dissolved in ethanol: dipped in each solution for 3 min.

$$SeO_2 + NaBH_4 + 6C_2H_5OH \rightarrow Se^{2-} + 2Na^+ + 2B(OC_2H_5)_3 + 5H_2 + 2H_2O$$

[24].

We repeated the SILAR cycle 3 times (denoted with "CdSSe3"). For the deposition of CdSe subsequently next to CdS layer, 0.40M Cd $(NO_3)_2 \cdot 4H_2O$

dissolved in ethanol and 0.40M SeO_2 dissolved in ethanol were prepared under inert N_2 atmosphere. The TiO_2 nanotubes electrode deposited with CdS were dipped into 0.40M SeO_2 dissolved in ethanol and 0.40M Cd $(NO_3)_2 \cdot 4H_2O$ dissolved in ethanol for 3 min, respectively. Then it was washed and dried. We repeated it 10 times (denoted with "CdSe10"). For the protection of our solar cell from the photocorrosion and the prevention of carrier recombination, ZnS capping layer finally was deposited. 0.50M $ZnSO_4 \cdot 7H_2O$ dissolved in ethanol and 0.50M $Na_2S \cdot 5H_2O$ dissolved in ethanol were prepared. Then it was washed and dried it in an oven at 50℃ for 3min under ambient air condition. We dipped the TiO_2 nanotubes photoelectrode deposited with ZnS/CdSSe/CdS into each solution prepared for 2min. All of the samples prepared were put into a quartz tube with a diameter of 3.15cm and then located in the center of horizontal tube furnace. We heated it for 1h at 450℃ and then let it cooled down naturally to room temperature.

3.5. Electrolyte Solution.

Photoelectrochemical process was carried out in a solution containing 0.35M Na_2SO_3 and 0.24M Na_2S in DI water where the polysulfide electrolyte was used. We used a three-electrode configuration consisting of the as-prepared sample photoelectrode as a working electrode (active area, 0.13 cm^2), a platinum mesh as a counter electrode, and a saturated Ag/AgCl electrode as a reference electrode were shown in Figure 3.2.

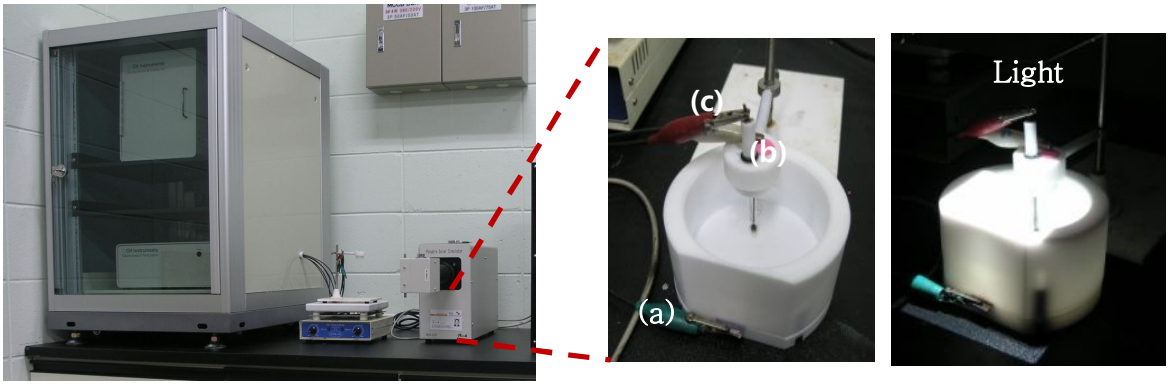

Fig 3.2 Three-electrode set up: (a) working electrode, (b) counter electrode and (c) reference electrode

3.6. Characterization and Measurement of the Materials.

The anodization current with time was automatically monitored using a digital multimeter (34401A, HP) interfaced with a notebook computer. The surface morphologies of the samples were characterized by a field-emission scanning electron microscope (Carl Zeiss, SUPRA 55VP). The top and side view measurements to observe the crystallinity of the sample were made at a 300 kV high-resolution transmission electron microscope (JEOL, JEM-3000F). Analytical TEM (FEI, Tecnai F20) operated at 200kV was used to observe the arrangement of TiO_2 nanotubes. The absorption spectra were obtained by a diffuse reflectance UV-Vis spectrophotometer (cary 5000, varian). The crystal structure patterns were obtained using a monochromatic Cu Kα radiation (λ = 1.54 Å) in the 2Θ angle range of 20° to 80° with X-ray diffractometer (D8-Advance, Bruker). The J-V curves were obtained with a solar simulator (Oriel 91160) at intensity of 100 mW/cm^2 (equivalent to one sun at AM1.5 filter) and a potentiostat

(Potentiostat/Galvanostat, EG&G 2634A). The prepared electrodes were anodically polarized from 1.0 V to -1.0 V at a scan rate of 5 mV/s.

CHAPTER 4. Results and Discussion

4.1. Experimental Scheme.

The general experimental scheme we take to produce the photo electrode made with the regular array of TiO_2 nanotubes anchored with ZnS/CdSSe/CdS quantum dot layers is given in Scheme 4.1. The energy structure associated with the materials used is also shown in Scheme 4.1

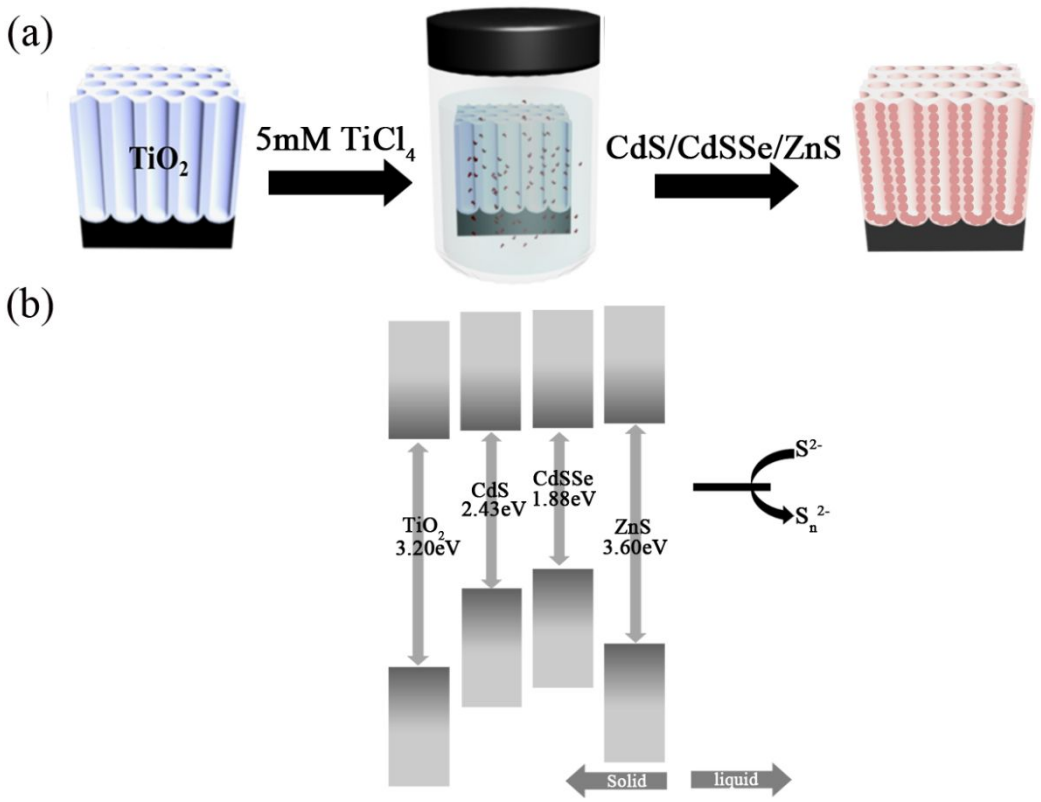

Scheme 4.1. Schematic diagram illustrating (a) the production of the photoelectrode, ZnS/CdSSe/CdS/TiO_2 NTs, (b) energy structures of the materials used for the efficient transport of photogenerated electrons and holes in a (ZnS/CdSSe/CdS)-sensitized TiO_2 nanotubes photoelectrode.

4.2. Morphology of the regular array of TiO_2 nanotubes surface-treated with $TiCl_4$ in various concentrations.

The regular array of TiO_2 nanotubes with a high crystallinity and free of surface defects were desirable as the photoelectrode for the solar energy conversion. The surface treatment of the regular array of TiO_2 nanotubes with $TiCl_4$ [32-34] was known to induce new TiO_2 growth on the preexisting metal oxide so that surface defective oxide tubes were cured. The surfaces of TiO_2 nanotubes were treated with $TiCl_4$ and then thermally annealed. As shown in Figure 4.1 (a) and (b), the channel walls of TiO_2 nanotubes treated with $TiCl_4$ were smoother and more crystalline than those untreated. The optimal length of TiO_2 nanotubes for solar energy conversion is known to be 20μm with the consideration of efficeint collection of electrons without any absorption loss [35]. Thus, we grew TiO_2 nanotubes of about 20μm in length. The HR-TEM images of TiO_2 nanotubes untreated with $TiCl_4$ or treated with $TiCl_4$ together with SEAD

(selected area electron diffraction) patterns were shown in Figure 4.1 (c) and (d), respectively. X-ray diffraction patterns of as-prepared TiO_2 nanotubes and TiO_2 nanotubes treated with 5mM $TiCl_4$ was given in Figure (e). Some particulates on the surface of TiO_2 nanotubes treated with $TiCl_4$ were noticeable. Some TiO_2 particles were grown onto it. With these data we could identify that it was anatase phase (JCPDS Card no. 21-1272; a = 3.785Å, c = 9.514Å).

From the SEAD patterns, we knew that a lot of aggregated polycrystalline $TiCl_4$ on the surface of TiO_2 nanotubes existed. The structural defects and cracks in TiO_2 nanotubes which disrupt the flow of electrons were removed by the surface passivation with $TiCl_4$ [34, 37]. The newly grown crystals of TiO_2 through the surface passivation with $TiCl_4$ were formed next to preexsiting TiO_2 nanotubes as shown in Figure 4.1 [38].

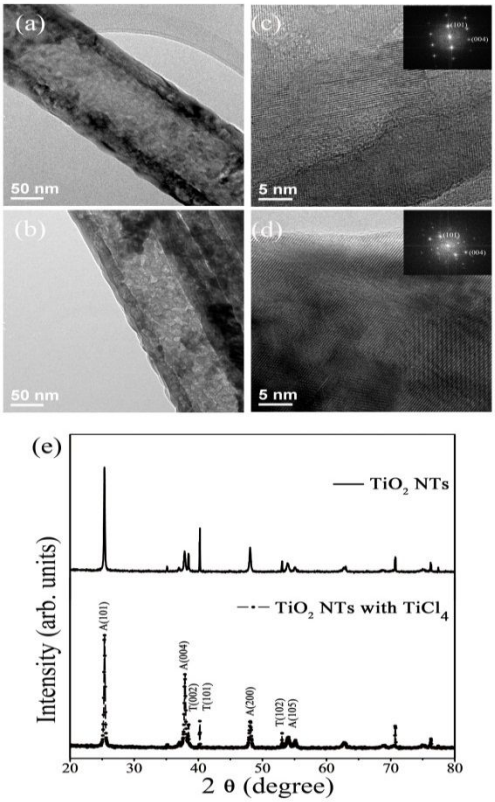

Fig 4.1 TEM images of the annealed TiO_2 nanotubes (a) untreated with $TiCl_4$, (b) treated with $TiCl_4$. (c) and (d) HR-TEM and SAED patterns of the TiO_2 nanotubes untreated with $TiCl_4$ or treated with $TiCl_4$, respectively. (e) X-ray diffraction patterns of as-prepared TiO_2 nanotubes and TiO_2 nanotubes treated with 5mM $TiCl_4$. A means anatase of TiO_2 and T means Ti metal itself.

4. 3. Synthesis of the TiO_2 nanotubes coupled with CdS, CdSSe.

To enhance the solar energy conversion efficiency, coupling TiO_2 nanotubes with a low band gap semiconductor material such as CdS, CdSSe were made. The photoactivity of TiO_2 NTs sensitized with CdS has been reported to be enhanced [36]. Adjusting the composition variable x in ternary CdS_XSe_{1-X} ($0 \leq x \leq 1$) alloy semiconductor, we tune its band gap to the desirable value with the reference to Vegard's law [39]. We varied the composition (i.e., x value) in CdS_XSe_{1-X} ($0 \leq x \leq 1$) alloy in terms of the molar S/Se ratio of the precursors and the band gap of CdSSe desired [15, 40, 41]. Another good property with CdS and ternary CdSSe alloy was of roughly identical onset potential -0.67 V vs Ag/AgCl. We prepared 6 different ternary Cd(Y)S(X)Se alloy [(Y, X): (0.2M, 0.1M), (0.2M, 0.2M), (0.2M, 0.3M), (0.1M, 0.2M), (0.2M, 0.2M), (0.3M, 0.2M)] anchored in the channel of TiO_2 nanotubes (length, L = ~20μm) grown on a flat Ti sheet by controlling the molar S/Se ratio of precursors. In order to produce

Cd(Y)S(X)Se/TiO_2 NTs, we dipped TiO_2 NTs treated with $TiCl_4$ into each solution containing each precursor ion for the 3 minutes of reaction and repeated 3 SILAR cycles. The UV-Vis absorption diffused reflectance spectra of CdS/ TiO_2 NTs, CdSe/ TiO_2 NTs, and Cd (Y)S (X)Se/TiO_2 NTs photoelectrodes were given in Figure 4.2. The absorption edges of CdS/ TiO_2 NTs and CdSe/ TiO_2 NTs, photoelectrodes appear at 2.48eV (500nm) and 1.72eV (718nm), respectively. Those of Cd(Y)S(X)Se/TiO_2 NTs photoelectrodes with Y=0.2M, X=0.1, 0.2, 0.3M were 1.98eV (626nm), 1.92eV (645nm), and 1.88eV (658nm), respectively.

With Se-richer than S in ternary CdSSe alloy as in Cd 0.2MS0.3MSe, its absorption edge gets more red shifted. So we were able to tune the band gap via composition variation in the unit of molar concentration(M) [42]. The TEM images in Figure 4.3 reveal the rough surface morphology of CdSSe /TiO_2 NTs photoeelctrode (length = ~20μm) on a flat Ti sheet. The ternary CdSSe alloy was overcoated all over the TiO_2 NTs and was not evenly distributed over the surface. The CdSSe QDs on TiO_2 NTs

were crystallized and had similar structures of the bulk CdS and CdSe (JCPDS Card no. 41-1049; a = 4.141Å, c = 6.720Å; JCPDS Card no. 75-5681; a = 4.298Å, c =7.008Å, respectively). The elemental mapping profile across the Cd (Y=0.2M)S (X=0.3M)Se /TiO_2 NTs photoelectrode confirms that the photoelectrode indeed consist of CdSSe QDs on TiO_2 NTs. The element analysis for multi-elements Ti, O, Cd, S, and Se was shown in Figure 4.3 (c) to (h). Ti and O elements were located in the whole part of the TiO_2 nanotubes whereas Cd, S, and Se elements were located randomly on the nanotubes and exist in much lower quantities.

To find the optimized ternary composition, we measured current-voltage characteristics of Cd (Y)S (X)Se /TiO_2 NTs treated with $TiCl_4$ phtoelectorde with various compositions. It was shown in Figure 4.4. Figure 4.4 (a) and (b) were current-voltage characteristics of Cd (Y=0.1, 0.2, 0.3M) S (X=0.2M)Se /TiO_2 NTs treated with $TiCl_4$ photoelectorde and Cd (Y=0.2M)S (X=0.1, 0.2, 0.3M)Se /TiO_2 NTs treated with $TiCl_4$ phtoelectorde, respectively. It turned out that the Cd (Y=0.2M)S

(X=0.3M)Se/TiO_2 NTs photoelectrodes was found to be the highest efficiency. The optimized composition of ternary Cd(Y)S(X)Se alloy is Cd (0.2M)S (0.3M)Se. Applied potential was measured with respect to an Ag/AgCl reference electrode.

Several groups examined the co-sensitization of CdS and CdSe or CdTe nanocrystals on TiO_2 or ZnO nanorods. The stacked layers of CdS and CdSe were made on the TiO_2 or ZnO nanorods by chemical evaporation method [42-44]. In order to achieve efficient QD-sensitized TiO_2 NTs photoelectrode, the band arrangement of QDs-TiO_2 NTs should be a ladder-like energy structure suitable for carrier transfer in the electrolyte solution. With the optimal Cd (0.2M)S (0.3M)Se alloy composition, we fabricated the photoelectrode in which Cd (0.2M)S (0.3M)Se layer was located between CdS and ZnS layers. As Se content increases in Cd 0.2MS (X)MSe (X= 0.1, 0.2, and 0.3), J_{SC} (short-circuit current) increases. Cd (Y)S (X)Se alloy with Se-richer than S was more efficient due to more photon absorption. The additional insertion of ternary Cd (Y)S (X)Se alloy layer

between CdS and CdSe was beneficial. To check whether the additional CdSe layer after the CdSSe layer deposition was beneficial, we carried out different number of SILAR cycles (n=3, 5, 8) to deposit CdSe layers next to CdSSe layer. We denote it with CdSe (n=3, 5, or 8). It was shown Figure 4.5. The additional CdSe layer deposition does not make any beneficial effect on photocurrent as shown in the top of Figure 4.5. The bottom part of Figure 4.5 showed the FESEM images of Ti/TiO_2 NTs/ CdS/ CdSSe/ CdSe (n=3,5,8) photoelectrodes, the deposition sequence of QD layers on the Ti/TiO_2 NTs was from the left to the right. FESEM images clearly show the deposition of QDs on TiO_2 NTs.

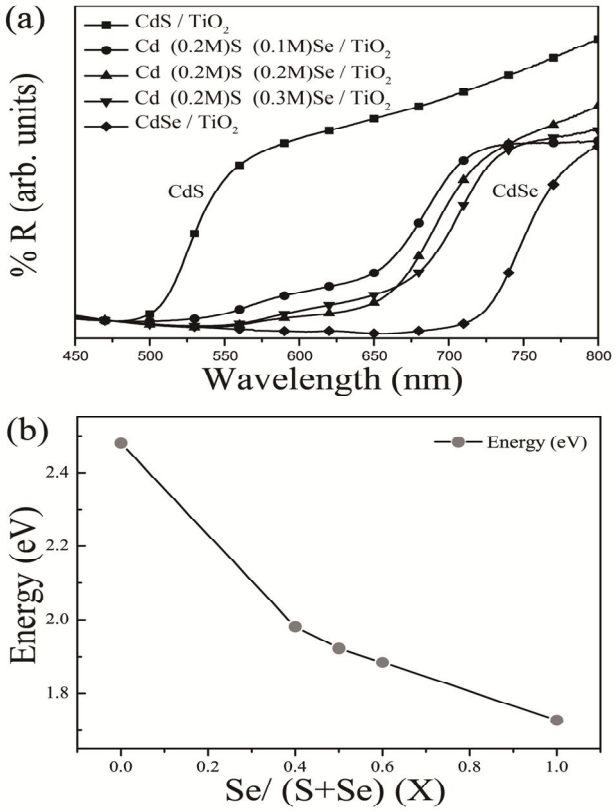

Fig 4.2 (a) UV-Vis absorption diffuse reflectance spectra of CdS, Cd(0.2M)S (X)Se (X = 0.1, 0.2, and 0.3M), and CdSe sensitized TiO_2 NTs photoelectrode, (b) Estimated band gap using Vegard`s law at different composition (X).

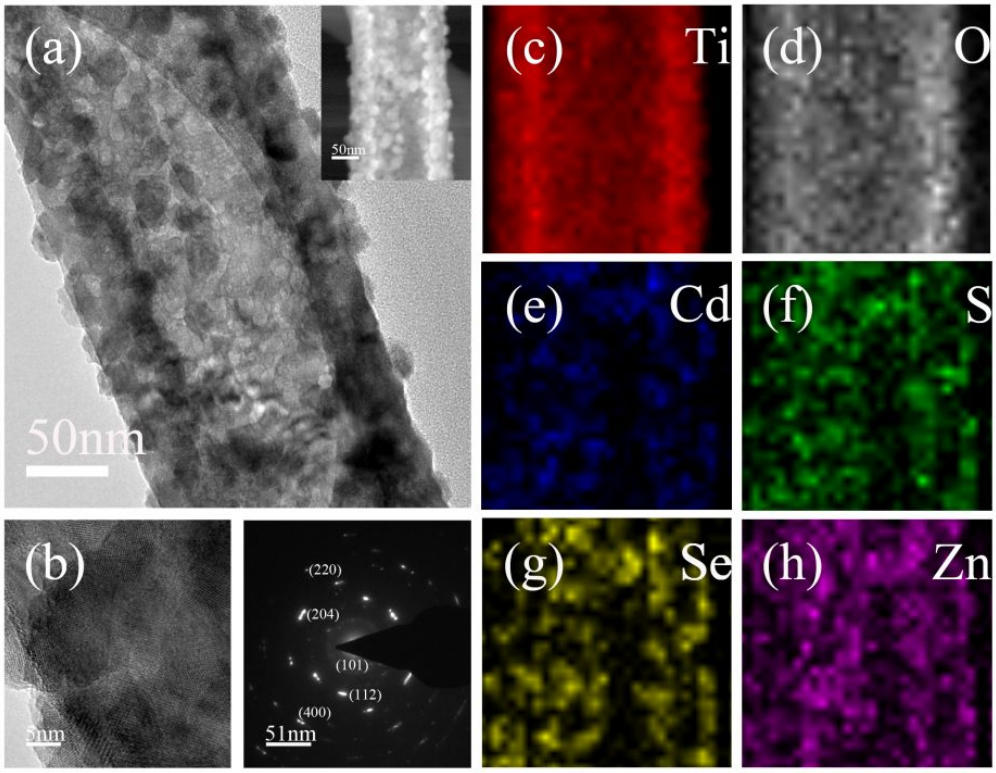

Fig 4.3 (a) TEM images of QDs-TiO_2 NTs (b) HR-TEM image and SAED patterns of CdSSe QDs on TiO_2 NTs photoelectrode, and (c)-(h) elemental mapping of CdSSe QDs on TiO_2 NTs photoelectrode by STEM image scan.

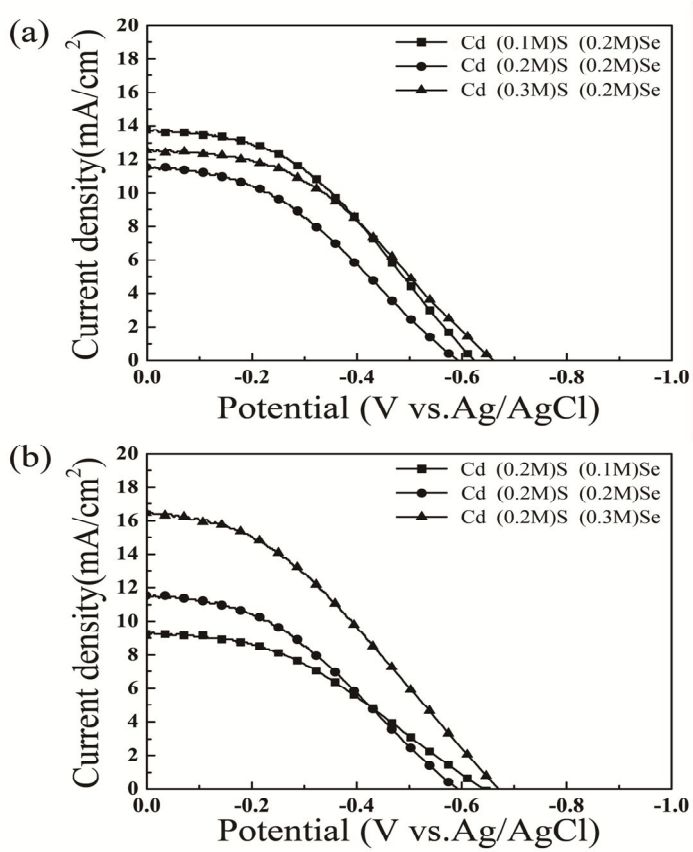

Fig 4.4 Current-Voltage characteristics of Cd(Y)S(X)Se /TiO_2 NTs treated with $TiCl_4$ photoelectrode, (a) Cd(Y=0.1, 0.2, 0.3M)S(X=0.2M)Se /TiO_2 NTs treated with $TiCl_4$ phtoelectorde. (b) Cd(Y=0.2M)S(X=0.1, 0.2, 0.3M)Se /TiO_2 NTs treated with $TiCl_4$ phtoelectorde

Concentration	V_{oc}(V)	J_{sc}(mA/cm^2)	FF	PCE (%)
Cd (0.2M)S (0.1M)Se	0.643	9.24	0.385	2.29
Cd (0.2M)S (0.2M)Se	0.594	11.5	0.378	2.59
Cd (0.2M)S (0.3M)Se	**0.671**	**16.5**	**0.360**	**3.98**
Cd (0.1M)S (0.2M)Se	0.624	13.8	0.412	3.53
Cd (0.2M)S (0.2M)Se	0.594	11.5	0.378	2.59
Cd (0.3M)S (0.2M)Se	0.661	12.6	0.412	3.43

Table 4.1 Electrochemical parameters of ternary Cd(Y)S (X)Se (Y=0.2M X=0.1, 0.2, 0.3M; Y=0.1,0.2, 0.3, X=0.2M) alloy deposited on the channel wall of TiO_2 nanotubes under light illumination.

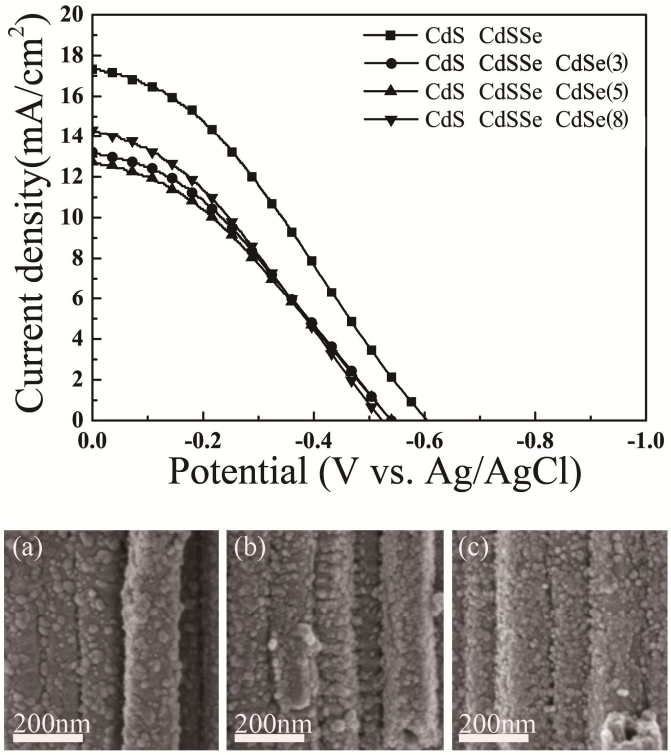

Fig 4.5 Current–Voltage characteristics (Top.) Field emission SEM images (Bottom) of the CdSe/CdSSe/CdS sensitized TiO_2 NTs photoelectrode with additional CdSe layer made through the # of SILAR clecles (n) : (a) CdSe3/CdSSe/CdS (n=3), (b) CdSe5 /CdSSe/CdS (n=5), and (c) CdSe8/ CdSSe/ CdS (n=8).

4.4 Optimal combination and sequence of QD layers on TiO_2 NTs array photoelectrode for better performance

The various combination and deposition sequences of QD layers on the TiO_2 NTs were performed and their I-V characteristics were measured to find out the best solar energy conversion photoelectrodes. As shown in Figure 4.6, A CdSSe/CdS sensitized TiO_2 NTs was more effective than CdSe /CdS sensitized and the final deposition of ZnS as a photocorrsion protecting layer on CdSSe/CdS/TiO_2 NTs (the deposition sequence was from right to left) was beneficial. The results altogether from Figures 4.4 to 4.6 indicate that Cd (0.2M)S (0.3M)Se was optimal composition for a ternary CdSSe alloy and that ZnS/CdSSe/CdS (The deposition sequence on TiO_2 NTs was from left to right.) was appropriate QD layers.

As summarized in Table 4.2, the PCE of the ZnS/CdSSe/CdS (the layer deposition sequence was form left to right) sensitized TiO_2 NTs photoelectrode was achieved as high as 4.67%. ZnS has the lattice

constant close to that of CdS and a wide band gap (Eg=3.6eV) [30], and thus serves as a proper photocorrosion protecting layer. The experimental result supports the photoelectrode capped with ZnS (PCE= 4.67%) had much higher PCE than that of the uncapped photoelectrode with ZnS(PCE=3.49%) under light illumination. The XRD patterns confirmed that the photoelectrode was indeed ZnS /CdSSe/ CdS /TiO_2 NTs/ Ti with wurtzite (220) ZnS at 2Θ=107.5°, (400) CdSe at 2Θ=111.7°, (112) CdS at 2 Θ=51.82°, and (101) TiO_2. The elemental mapping profile also reveals the photoelectrode was composed of Ti, O, Cd, S, Se, and Zn. Enhanced V_{oc} (open circuit voltage) and FF (fill factor) in ZnS /CdSSe/ CdS-sensitized TiO_2 NT/ Ti photoelectrode indicate that the charge recombination was suppressed and the photocorrosion reaction was prevented with ZnS capping layer deposited [28].

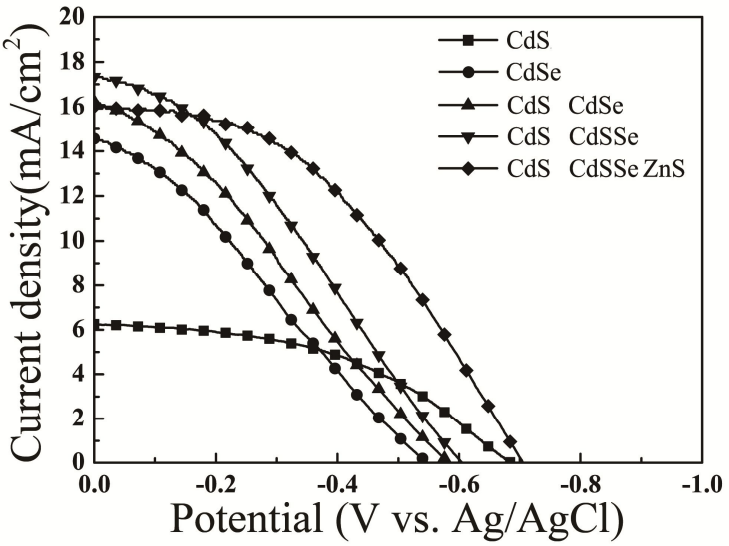

Fig 4.6 Current-Voltage characteristics of CdS, CdSe, CdS/CdSe (here, the deposition sequence of QDs on NTs is CdS, CdSe.), CdS/CdSSe (here, the deposition sequence of QDs on NTs is CdS, CdSSe.), and CdS/CdSSe/ZnS (here, the deposition sequence of QDs on NTs is CdS, CdSSe, and ZnS.) sensitized TiO_2 NTs photoelectrode.

Photoelectrode	V_{oc}(V)	J_{sc}(mA/cm^2)	FF	PCE (%)
CdS	0.686	6.25	0.456	1.96
CdSe	0.547	14.6	0.286	2.28
CdS/CdSe	0.586	16.2	0.295	2.81
CdS/CdSSe	0.606	17.3	0.333	3.49
CdS/CdSSe/ZnS	**0.707**	**16.0**	**0.413**	**4.67**

Table 4.2 Electrochemical parameters of CdS, CdSe, CdS/CdSe, CdS/CdSSe, and CdS/CdSSe/ZnS sensitized TiO_2 NTs photoelectrode under light illumination. Here the deposition sequence of CdS/CdSe, CdS/CdSSe, and CdS/CdSSe/ZnS on TiO_2 NTs/Ti photoelectrodes were (CdS→ CdSe), (CdS→CdSSe), and (CdS→CdSSe→ZnS), respectively.

CHAPTER 5. Conclusions

The photoelectrode fabricated with the regular array of TiO_2 nanotubes anchored with ZnS/CdSSe/CdS quantum dots was prepared by the following steps: 1) the formation of the regular array of TiO_2 nanotubes on a Ti metal sheet, 2) the surface treatment of the TiO_2 nanotubes with $TiCl_4$ for the removal of surface defect sites on NTs, 3) the sequential deposition of CdS, CdSSe, and ZnS, in situ, onto the channel walls of TiO_2 nanotubes by the successive ionic layer adsorption and reaction (SILAR) procedure. The tuning of the band gap of CdSSe was done in terms of controlling the composition of Cd, S, or Se during the SILAR procedure. In this way, a ladder-like energy structure suitable for carrier transfer was attained from ZnS/CdSSe/CdS through TiO_2 nanotubes to a Ti metal sheet. The more photoinduced charge carrier transfer from the quantum dots anchored on the TiO_2 nanotubes was achieved and thus, the solar energy conversion efficiency was enahnced. The power

conversion efficiency (PCE) of our solar cell fabricated with the regular array of TiO_2 nanotubes anchored with CdSSe/CdS or CdSe/CdS quantum dots was PCE = 3.49 % and 2.81 % under the illumination at 100 mW/cm^2, respectively. To protect the photocorrosion of our solar cell photoelectrode from the electrolyte and to suppress the carrier recombination, ZnS was introduced onto CdSSe/CdS. The power conversion efficiency (PCE) of our solar cell with the structure of a photoelectrode, (ZnS/CdSSe/CdS/TiO_2 NTs/ a Ti metal sheet) was 4.67 % under the illumination at 100 mW/cm^2

References

1. Karthik, S.; Gopal, K. M.; Haripriya, E. P.; Sorachon, Y.; Maggie, P.; Oomman, K. V.; Craig, A. G. *Nanotech.* 2007, 18, (6), 065707.

2. Shin, Y.; Lee, S. *Nano Lett.* 2008, 8, (10), 3171-3173.

3. Cheng, S.; Fu, W.; Yang, H.; Zhang, L.; Ma, J.; Zhao, H.; Sun, M.; Yang, L. *J. Phys.Chem. C* 2011, 116, (3), 2615-2621.

4. Yang, K.; Dai, Y.; Huang, B.; Whangbo, M.-H. *J. Phys. Chem. C* 2009, 113, (6), 2624-2629.

5. Ghicov, A.; Macak, J. M.; Tsuchiya, H.; Kunze, J.; Haeublein, V.; Frey, L.; Schmuki, P. *Nano Lett.* 2006, 6, (5), 1080-1082.

6. Long, R.; English, N. J.; Dai, Y. *J. Phys. Chem. C* 2009, 113, (40), 17464-17470.

7. W. Choi, A. Termin, and M. R. Hoffmann, J. Phys. Chem. 98 (1994), 13669.

8. M. Anpo and M. Takeuchi, J. Catal., 216, (2003), 505-516.

9. Sun, W.-T.; Yu, Y.; Pan, H.-Y.; Gao, X.-F.; Chen, Q.; Peng, L.-M. *J. Am. Chem. Soc.* 2008, 130, (4), 1124-1125.

10. Lee, Y.-L.; Huang, B.-M.; Chien, H.-T. *Chem. Mater.*2008, 20, (22), 6903-6905.

11. Seabold, J. A.; Shankar, K.; Wilke, R. H. T.; Paulose, M.; Varghese, O. K.; Grimes, C. A.; Choi, K.-S. *Chem. Mater.* 2008, 20, (16), 5266-5273.

12. Lee, H.; Leventis, H. C.; Moon, S.-J.; Chen, P.; Ito, S.; Haque, S. A.; Torres, T.; Nüesch, F.; Geiger, T.; Zakeeruddin, S. M.; Grätzel, M.; Nazeeruddin, M. K. *Adv.Funct. Mater.* 2009, 19, (17), 2735-2742.

13. Vogel, R.; Hoyer, P.; Weller, H. *J. Phys.Chem.* 1994, 98, (12), 3183-3188.

14. Yu-Jen, S.; Yuh-Lang, L. *Nanotech.* 2008, 19, (4), 045602.

15. Pan, A.; Yang, H.; Liu, R.; Yu, R.; Zou, B.; Wang, Z. *J. Am. Chem. Soc.* 2005, 127, (45), 15692-15693.

16. Pan, A. L.; Yao, L.; Qin, Y.; Yang, Y.; Kim, D. S.; Yu, R.; Zou, B.; Werner, P.; Zacharias, M.; Gø sele, U. *Nano Lett.* 2008, 8, (10), 3413-3417.

17. Johnston, J. W. D. *J. Appl. Phys.* 1971, 42, (7), 2731-2740.

1. Karthik, S.; Gopal, K. M.; Haripriya, E. P.; Sorachon, Y.; Maggie, P.; Oomman, K. V.; Craig, A. G. *Nanotech.* 2007, 18, (6), 065707.

2. Shin, Y.; Lee, S. *Nano Lett.* 2008, 8, (10), 3171-3173.

3. Cheng, S.; Fu, W.; Yang, H.; Zhang, L.; Ma, J.; Zhao, H.; Sun, M.; Yang, L. *J. Phys.Chem. C* 2011, 116, (3), 2615-2621.

4. Yang, K.; Dai, Y.; Huang, B.; Whangbo, M.-H. *J. Phys. Chem. C* 2009, 113, (6), 2624-2629.

5. Ghicov, A.; Macak, J. M.; Tsuchiya, H.; Kunze, J.; Haeublein, V.; Frey, L.; Schmuki, P. *Nano Lett.* 2006, 6, (5), 1080-1082.

6. Long, R.; English, N. J.; Dai, Y. *J. Phys. Chem. C* 2009, 113, (40), 17464-17470.

7. W. Choi, A. Termin, and M. R. Hoffmann, J. Phys. Chem. 98 (1994), 13669.

8. M. Anpo and M. Takeuchi, J. Catal., 216, (2003), 505-516.

9. Sun, W.-T.; Yu, Y.; Pan, H.-Y.; Gao, X.-F.; Chen, Q.; Peng, L.-M. *J. Am. Chem. Soc.* 2008, 130, (4), 1124-1125.

10. Lee, Y.-L.; Huang, B.-M.; Chien, H.-T. *Chem. Mater.*2008, 20, (22), 6903-6905.

11. Seabold, J. A.; Shankar, K.; Wilke, R. H. T.; Paulose, M.; Varghese, O. K.; Grimes, C. A.; Choi, K.-S. *Chem. Mater.* **2008,** 20, (16), 5266-5273.

12. Lee, H.; Leventis, H. C.; Moon, S.-J.; Chen, P.; Ito, S.; Haque, S. A.; Torres, T.; Nüesch, F.; Geiger, T.; Zakeeruddin, S. M.; Grätzel, M.; Nazeeruddin, M. K. *Adv.Funct. Mater.* **2009,** 19, (17), 2735-2742.

13. Vogel, R.; Hoyer, P.; Weller, H. *J. Phys.Chem.* **1994,** 98, (12), 3183-3188.

14. Yu-Jen, S.; Yuh-Lang, L. *Nanotech.* **2008,** 19, (4), 045602.

15. Pan, A.; Yang, H.; Liu, R.; Yu, R.; Zou, B.; Wang, Z. *J. Am. Chem. Soc.* **2005,** 127, (45), 15692-15693.

16. Pan, A. L.; Yao, L.; Qin, Y.; Yang, Y.; Kim, D. S.; Yu, R.; Zou, B.; Werner, P.; Zacharias, M.; Go·sele, U. *Nano Lett.* **2008,** 8, (10), 3413-3417.

17. Johnston, J. W. D. *J. Appl. Phys.* **1971,** 42, (7), 2731-2740.

18. Hurwitz, C. E. *Appl. Phys. Lett.* **1966,** 8, (10), 243-245.

19. Zaban, A.; Mićić, O. I.; Gregg, B. A.; Nozik, A. J. *Langmuir* **1998,** 14, (12), 3153-3156.

20. Leschkies, K. S.; Divakar, R.; Basu, J.; Enache-Pommer, E.; Boercker, J. E.; Carter, C. B.; Kortshagen, U. R.; Norris, D. J.; Aydil, E. S. *Nano Lett.* **2007,** 7, (6), 1793-1798.

21. Robel, I.; Subramanian, V.; Kuno, M.; Kamat, P. V. *J. Am. Chem. Soc.* **2006,** 128, (7), 2385-2393.

22. Chang, C.-H.; Lee, Y.-L. *Appl. Phys. Lett.* **2007,** 91, (5), 053503-3.

23. Nicolau, Y. F. *Appl. Surf. Sci.* **1985,** 22–23, Part 2, (0), 1061-1074.

24. Lee, H.; Wang, M.; Chen, P.; Gamelin, D. R.; Zakeeruddin, S. M.; Gra·tzel, M.; Nazeeruddin, M. K. *Nano Lett.* **2009,** 9, (12), 4221-4227.

25. Lee, H. J.; Bang, J.; Park, J.; Kim, S.; Park, S.-M. *Chem. Mater.* **2010,** 22, (19), 5636-5643.

26. Guijarro, N. s.; Lana-Villarreal, T.; Mora-Sero·, I. n.; Bisquert, J.; Go·mez, R. *J. Phys. Chem. C* **2009,** 113, (10), 4208-4214.

27.Sven Rühle, Menny Shalom, and Arie Zaban, ChemPhysChem 2010, 11, 2290, 25.

28. Diguna, L. J.; Shen, Q.; Kobayashi, J.; Toyoda, T. *Appl. Phys. Lett.* **2007,** 91, (2), 023116-3.

29. Yang, S.-m.; Huang, C.-h.; Zhai, J.; Wang, Z.-s.; Jiang, L. *J. Mater. Chem.* **2002,** 12, (5), 1459-1464.

30. Spanhel, L.; Haase, M.; Weller, H.; Henglein, A. *J. Am. Chem. Soc.* 1987, 109, (19), 5649-5655.

31. Rho, C.; Min, J.-H.; Suh, J. S. *J. Phys. Chem. C* 2012, 116, (12), 7213-7218.

32. Hong, L.; Liang, T.; Wenzhong, S. *Nanotech.* 2011, 22, (15), 155603.

33. Ito, S.; Murakami, T. N.; Comte, P.; Liska, P.; Grätzel, C.; Nazeeruddin, M. K.; Grätzel, M. *Thin Solid Films* 2008, 516, (14), 4613-4619.

34. Liu, B.; Aydil, E. S. *J. Am. Chem. Soc.* 2009, 131, (11), 3985-3990.

35. Jennings, J. R.; Ghicov, A.; Peter, L. M.; Schmuki, P.; Walker, A. B. *J. Am. Chem. Soc.* 2008, 130, (40), 13364-13372.

36. Banerjee, S.; Mohapatra, S. K.; Das, P. P.; Misra, M. *Chem. Mater.* 2008, 20, (21), 6784-6791.

37. Zhu, K.; Vinzant, T. B.; Neale, N. R.; Frank, A. J. *Nano Lett.* 2007, 7, (12), 3739-3746.

38. Mor, G. K.; Shankar, K.; Paulose, M.; Varghese, O. K.; Grimes, C. A. *Nano Lett.* 2005, 6, (2), 215-218.

39. Laura A. Swafford et al., *J. Am. Chem. Soc.* 2006, *128,* 12299-12306.

40. Liang, Y.; Zhai, L.; Zhao, X.; Xu, D. *J. Phys. Chem. B* 2005, 109, (15), 7120-7123.

41. Swafford, L. A.; Weigand, L. A.; Bowers, M. J.; McBride, J. R.; Rapaport, J. L.; Watt, T. L.; Dixit, S. K.; Feldman, L. C.; Rosenthal, S. J. *J. Am. Chem. Soc.* 2006, 128, (37), 12299-12306.

42. Myung, Y.; Jang, D. M.; Sung, T. K.; Sohn, Y. J.; Jung, G. B.; Cho, Y. J.; Kim, H. S.; Park, J. *ACS Nano* 2010, 4, (7), 3789-3800.

43. Luo, J.; Ma, L.; He, T.; Ng, C. F.; Wang, S.; Sun, H.; Fan, H. J. *J. Phys. Chem. C* 2012, 116, (22), 11956-11963.

44. Sung, T. K.; Kang, J. H.; Jang, D. M.; Myung, Y.; Jung, G. B.; Kim, H. S.; Jung, C. S.; Cho, Y. J.; Park, J.; Lee, C.-L. *J. Mater. Chem.* 2011, 21, (12), 4553-4561.

국문초록

본 연구는 기존의 거친 표면 거칠기를 지니는 베어(bare) 타이타늄(즉, ~96nm의 rms) 기판을 이용하여 양극산화 방법으로 성장시킨 불규칙한 타이타늄 나노튜브의 단점을 해결할 수 있는 제조 방법 개발 및 성장 메커니즘 이해와 태양의 에너지(가시광선 영역: 380nm~750nm)를 효율적을 흡수할 수 있는 양자점(CdS, CdSSe, ZnS 등)을 만들고 이것을 응용하여 신소재 재료인 타이타니아(TiO_2)나노튜브에 적용시켜 태양에너지의 이해를 목적으로 연구는 진행 되었다. 평탄한 타이타늄 기판(즉, ~1nm의 rms)을 달성하기 위하여 전처리 과정으로 전해연마(electropolishing) 과정을 수행하였다. 이 평탄한 기판은 첫 번째 양극산화 과정이 진행 되는 동안 금속 표면에 전체적으로 균일한 전기장 분포를 보장하여 기판에 규칙적으로 수직 배향한 나노튜브의 성장을 유도하였다. 또한, 양극산화를 통해 제조한 타이타니아 층과 남아 있는 타이타늄 금속 계면의 약한 접착력에 착안하여 테이프 등을 이용하여 손쉽게 타이타니아 층을 제거함으로써 조밀 육방정(hexagona close-packing) 패턴을 가지는 타이타늄 금속 표면을 얻을 수 있었다. 이 기판을 이용하여 제조된 나노튜브 표면을 QDs (quantum dots: CdS, CdSSe and ZnS) sequential ionic bath deposition을 통해 완성한다. 각각을 이온상태로 만든 후 여러 번 증착 과정을 수행으로 흡수파장 영역을 넓혀가고 원하는 파장대에 맞는 크기를 얻게 되며 태양에너지를 포괄적을 이용한다.

TiO_2의 태양광의 흡수 영역대는 자외선 영역으로 태양에너지의 단 20% 정도 흡수를 하는 단점을 보완하기 위해 QDs로 태양광의 에너지의 흡수영역대를 확장 시키는 연구를 진행하며 태양에너지 및 전지의 이해 도울 수 있었다. 또한, QDs로 TiO_2가 흡수하지 못하는 가시광영역의 태양광을 흡수하므로써 효율증가값 (4.67%)에 도달할 수 있었다. 결론적으로 신기능성 TiO_2의 소재와 양자점을 접목시킨 태양전지 관련한 연구에 적용이 가능하다는 것을 알 수 있었다.

주요어: *TiO_2 나노튜브, 양자점, 연속 이온 증착, 태양 전지*

감사의 글

아낌없는 응원과 도움을 주신 교수님, 가족, 친구, 지인 분들께. 진심으로 감사의 말씀 드립니다. 과분하게 받은 사랑을 잊지 않고 언제나 베풀면서 살아갈 수 있는 사람이 되도록 하겠습니다. 감사합니다.